Title:

In Silico Analysis of Inner Ear Development using Public Whole Embryonic Body Single-Cell RNA-sequencing Data

Ryosuke Yamamoto [a]; Hiroe Ohnishi [a]; Koichi Omori [a]; Norio Yamamoto [a]*

[a] Department of Otolaryngology, Head and Neck Surgery, Graduate School of Medicine, Kyoto University, 54, Shogoin Kawahara-cho, Sakyo-ku, Kyoto, 6068507, Japan

Ryosuke Yamamoto: e-mail address, r_yamamoto@ent.kuhp.kyoto-u.ac.jp; phone numbers, +81-75-751-3346

Hiroe Ohnishi: e-mail address, h_oonishi@ent.kuhp.kyoto-u.ac.jp; phone numbers, +81-75-751-3346

Koichi Omori: e-mail address, omori@ent.kuhp.kyoto-u.ac.jp; phone numbers, +81-75-751-3346

*Norio Yamamoto: e-mail address, yamamoto@ent.kuhp.kyoto-u.ac.jp; phone number, +81-75-751-3346

Corresponding author: Norio Yamamoto

Department of Otolaryngology, Head and Neck Surgery, Graduate School of Medicine, Kyoto University, 54, Shogoin Kawahara-cho, Sakyo-ku, Kyoto, 6068507, Japan

E-mail address: yamamoto@ent.kuhp.kyoto-u.ac.jp

Abstract

The inner ear comprises four epithelial domains: the cochlea, vestibule, semicircular canals, and endolymphatic duct/sac. These structures are segregated at embryonic day 13.5 (E13.5). However, these four anatomical structures remain undefined at E10.5. Here, we aimed to identify lineage-specific genes in the early developing inner ear using published data obtained from single-cell RNA-sequencing (scRNA-seq) of embryonic mice. We downloaded 5,000 single-cell transcriptome data, named ‘auditory epithelial trajectory’, from the Mouse Organogenesis Cell Atlas. The dataset was supposed to include otic epithelial cells at E9.5–13.5. We projected the 5,000 cells onto a two-dimensional space encoding the transcriptional state and visualised the pattern of otic epithelial cell differentiation. We identified 15 clusters, which were annotated as one of the four components of the inner ear epithelium using known genes that characterise the four different tissues. Additionally, we classified 15 clusters into sub-regions of the four inner ear components. By comparing transcriptomes between these 15 clusters, we identified several candidates of lineage-specific genes. Characterising these new candidate genes will help future studies about inner ear development.

Abstract: 175 words

Keywords: embryonic development; inner ear; otic vesicle; RNA-sequencing; single-cell analysis

1. Introduction

Until recently, comprehensive analysis of gene expression was performed using whole tissues. However, transcriptome analysis that can be performed at the tissue level does not reflect the diversity of each cell within the organ and thus, is not suitable for lineage analysis of differentiating cells, especially in organs such as the inner ear, where adjacent cells are differentially matured cells. Single-cell RNA-sequencing (scRNA-seq), which provides comprehensive information on gene expression at the single-cell level, has become widespread and has helped discover undefined cell sub-populations during the developmental and mature stages of various organs (Shapiro et al., 2013; Treutlein et al., 2014; Zeisel et al., 2015). Using scRNA-seq, it is possible to detect subtypes of cells within a group of cells that have been conventionally considered to be uniform from a morphological viewpoint, based on their different gene expression patterns. Hence, single-cell analysis is a revolutionary research method for the study of cell differentiation and fate determination.

The inner ear has multiple sensory organs, providing us with hearing and balance sensation. There are three kinds of end organs in the inner ear: the organ of Corti, the macula, and the crista. The organ of Corti is a part of the cochlea, responsible for sound detection. Non-sensory epithelia are located medial and lateral to the organ of Corti within the cochlear duct. As the cochlear duct coils around the modiolus, where the cell bodies of spiral ganglion cells (primary auditory neurons) exist, the medial non-sensory epithelia of the cochlea are found between the organs of Corti and the cochlear modiolus. The macula is the sensory organ of the vestibule, which also includes the saccule and the utricle, and detects the head tilt and linear acceleration. The crista is the sensory organ of the semicircular canals, detecting rotational movements. The sensory

epithelia of the mammalian inner ear are unable to physiologically regenerate after birth. As a result, the sensorineural hearing loss caused by the impairment of the cochlear sensory epithelia is intractable. Although several studies have tried to regenerate the cochlear sensory epithelia from induced pluripotent stem cells (Ohnishi et al., 2015; Oshima et al., 2010), the efficiency is poor probably due to a lack of knowledge regarding the development of the inner ear.

In mice, the development of the inner ear starts around embryonic day 8.0–8.5 (E8.0–8.5) as a placodal thickening of the head ectoderm, called the otic placode. The otic placode then invaginates to form an otic cup, quickly separating from the adjacent ectoderm to form a closed, single-cell thick, spherical vesicle, the otic vesicle (Sai and Ladher, 2015). The four anatomical structures, the cochlea, the vestibule, the semicircular canals, and the endolymphatic duct/sac are visibly and morphologically segregated at E12–13. Although these four structures and their boundaries remain unclear in the otic vesicle at E10.5, the region from which each structure has originated can be determined at this stage (Fig. 1) (Li et al., 1978). The cochlear duct is known to be derived from the ventral half of the otic vesicle, while the origin of the vestibule is the ventral-to-middle part of the otic vesicle. In contrast, the semicircular canal, is known to arise from the dorso-lateral part of the otic vesicle, while the endolymphatic duct is formed at the dorso-medial part of the otic vesicle (Brigande et al., 2000).

Despite its small size, the inner ear contains various cells arranged in a complicated way at a single-cell level. Therefore, it is reasonable to apply scRNA-seq or single-cell quantitative RT-PCR in studies of the inner ear development. For example, Burns et al. applied scRNA-seq to reveal the heterogeneity of the sensory organs of the cochlea and the vestibule in neonatal mice (Burns et al., 2015). Likewise, Durruthy-Durruthy et al.

investigated the mouse otic vesicle and early neuroblast lineage at single-cell resolution using quantitative RT-PCR (Durruthy-Durrthy et al., 2014). They subdivided the otic vesicle into distinct octants and established a 3D otic vesicle model based on the expression profile of 96 genes. However, the heterogeneity of the otic vesicle at the transcriptome level remains unknown. Using 2,000,000 single-cell transcriptomes, Cao et al. identified 10 major developmental trajectories and 56 sub-trajectories in the embryonic mouse development (Cao et al., 2019). One of the sub-trajectories is “Auditory epithelial trajectory”, which included three populations named as "Otic vesicle epithelium", "Otic sensory epithelium", and "Utricle and saccule epithelium". However, they did not analyse these populations in detail. Hence, we thought that the three clusters are not sufficient to explain the heterogeneity of the otic epithelial cells, and changes in the gene expression during the development of the inner ear had also not been clarified. In this study, in order to obtain sufficient knowledge to induce the mammalian sensory epithelia of the inner ear, we elucidated the cell-fate specific gene expression patterns in the early developing inner ear using published data obtained by scRNA-seq.

2. Materials and Methods

2.1. Downloading single-cell transcriptome data of the auditory epithelial trajectory from the Mouse Organogenesis Cell Atlas

In February 2019, Cao et al. published the transcriptome data of two million whole-body cells collected from E9.5–13.5 mice (Cao et al., 2019). They profiled the RNA in nuclei using sci-RNA-seq 3. These profiles might therefore primarily reflect nascent transcription, temporally offset, but also predictive of the cellular transcriptome

(La Manno et al., 2018). Despite shallow sequencing (about 5,000 raw reads per cell), they recovered a median of 671 unique molecular identifiers (UMI), detected 519 genes per cell, and selected cells whose UMI counts were more than 400. Putative doublet cells were excluded from the analysis using Scrublet (Wolock et al., 2019). These single-cell transcriptomes were then subjected to Louvain clustering and UMAP visualisation, and 56 developmental trajectories were identified. Cao et al. defined three auditory epithelial trajectories from epithelial cell clusters that were defined by the expression of Epcam, Trp63, and Grhl2. The defining markers of these three auditory epithelial trajectories were Otol1, Oc90, and Nox3, respectively. We downloaded the filtered matrices of the counts defined as an auditory epithelial trajectory (5,000 cells and 12,354 genes) from the Mouse Organogenesis Cell Atlas (https://oncoscape.v3.sttrcancer.org/atlas.gs.washington.edu.mouse.rna/downloads), along with metadata (e.g. developmental stage) for each barcode. The 5,000 cells were shown to have a median of 805 UMI and 614 genes per cell.

2.2. Analysis method

We analysed the transcriptome of the 5,000 cells using Seurat 3.1.1 library on R 3.6.2 (Hoffman et al., 2018; Stuart et al., 2019). The dataset was normalised using R package sctransform, which included the selection of variable genes (Hafemeister and Satija, 2019). During normalisation, we also corrected for cell cycle bias. We performed principal component analysis (PCA) to reduce dimensionality on the normalised data matrix. For PCA, we used the top 2,000 most highly variable genes. We kept the first 15 PCs based on eigenvalue drop-off. For 2D visualisation, PC embeddings were passed into UMAP (McInnes et al., 2018). The parameters for UMAP were as follows: min_dist = 0.01, n (the number of neighbours) = 15. We applied the Louvain clustering

algorithm for community detection. The Seurat FindMarkers function was used to explore marker genes for the clusters (Wilcoxon rank-sum test, adjusted p-value < 0.01, log-fold-change threshold > 0.1) (Supplementary table). The clusters were annotated based on established marker genes (Table 1). During analyses of differentially expressed genes (Table 2), we used Wilcoxon rank-sum test and we set a log-fold-change threshold > 0.25 and adjusted p-value < 0.05. P-value was adjusted by Bonferroni correction.

2.3. Animals

We purchased Slc:ICR mice from Japan SLC, Inc (Hamamatsu, Japan). All experiments were performed in accordance with the National Institutes of Health Guidelines for the Care and Use of Laboratory Animals, and were approved by the Animal Research Committee of Kyoto University Graduate School of Medicine. (MedKyo19536; Kyoto, Japan)

2.4. In Situ Hybridisation (ISH)

Whole embryos (E9.5 and 10.5) and whole heads (E11.5, 12.5, and 13.5) were fixed by immersion in 4 % paraformaldehyde (PFA, Nacalai Tesque, Kyoto, Japan) for 16 h at 4 °C. After adjusting the osmotic pressure with 15 and 30 % sucrose/PBS (Nacalai Tesque), respectively, overnight, tissues were embedded in Tissue-Tek® O.C.T.™ compound (Sakura Finetek, Tokyo, Japan) and frozen at −80 °C. We mounted frozen sections (12 μm thick) on silane-coated slide glasses (Matsunami Glass, Osaka, Japan). Probes used for in situ hybridisation were as follows; *Adamtsl1* (NM_029967.3, nucleotides 2,949–3,907), *Ebf1* (NM_001290709, nucleotides 1,436–2,269), *Elf1*

(NM_001286411.1 nucleotides 1,136–2,164), *Rorb* (NM_001043354.2 nucleotides 1,284–2,307), *Sox2* (IMAGE clone: 6413283), *Vav3* (NM_020505.2 nucleotides 3,981–4,914), and *Zpld1* (NM_178720.4 nucleotides 859–1,725).

We generated cDNA fragments by PCR from E13.5 mouse inner ear cDNA and cloned them into the pCR™-Blunt II-TOPO® vector (Invitrogen, New York, USA). Probes were synthesised using the DIG RNA Labeling Kit (Roche, Basel, Switzerland) after digestion with BamHI-HF, HindIII, NotI-HF, SacI, or XhoI (New England Biolabs, Massachusetts, USA). Before hybridisation, sections were re-fixed with 4 % PFA and 0.2 % glutaraldehyde (Nacalai Tesque), bleached with 6 % hydrogen peroxidase (FUJIFILM Wako Pure Chemical Corporation, Osaka, Japan) treated with proteinase K (20 μg/μL, Roche) for 2.5 min, and re-fixed. Sections were then incubated in pre-hybridisation solution (50 % formamide [Nacalai Tesque], 5× Saline Sodium Citrate Buffer [SSC, Nacalai Tesque; adjusted to pH 4.5 with citrate], 1 % sodium dodecyl sulfate [SDS, Sigma-Aldrich, Missouri, USA], 50 μg/mL yeast RNA [Invitrogen], and 50 μg/mL heparin [Sigma-Aldrich]) at 65 °C for 1 h. Next, DIG-labelled RNA probes were hybridised to sections at 65 °C for 16 h. After transferring into Tris-buffered saline (TBS, Nacalai Tesque), sections were blocked with 5 % sheep serum (Sigma-Aldrich), and incubated with a 1:4,000 dilution of Anti-Digoxigenin-AP, Fab fragments (Roche) at 4 °C overnight. To detect the hybridised probes, slides were dipped in nitro-blue tetrazolium chloride (Roche) and 5-bromo-4-chloro-3-indolyl phosphate solution (Roche). Sections were photographed using a BX-50 microscope (Olympus, Tokyo, Japan).

3. Results

3.1. Uniform Manifold Approximation and Projection (UMAP) visualisation of the 5,000 otic epithelial cells and clustering

We utilised published transcriptome data of two million whole-body cells collected from E9.5–13.5 mice (Cao et al., 2019). Data contained a subset of cells defined as an auditory epithelial trajectory, regarded as being of an otic epithelial lineage (see methods), which expressed three epithelial cell markers (Epcam, Trp63, and Grhl2) and one of three otic markers (Oc90, Nox3, or Otol1). This subset was composed of 5,000 cells from five embryonic stages (E9.5, 10.5, 11.5, 12.5, and 13.5) with a median of 805 unique molecular identifiers (UMI) and 614 genes per cell. We subjected the 5,000 single-cell transcriptomes to Louvain clustering and UMAP visualisation (Figs. 2, 3) (McInnes et al., 2018). Applying the Louvain clustering algorithm for community detection, we identified 15 clusters, whose distribution is indicated with different colours in the UMAP visualisation in Fig. 2. The same UMAP visualisation showing only cells from each stage (E9.5: 710 cells; E10.5: 1,037 cells; E11.5: 1,662 cells; E12.5: 888 cells; E13.5: 703 cells) is plotted in Fig. 3. Notably, E9.5 cells are located at the centre of the plot. With the proceeding of the developmental stages, cells are shown to be distributed at the outer place within the plot. We also produced a heatmap representing the expression levels of the top 30 marker genes (y-axis) for each cluster (x-axis), sorted in the order of the larger fold change observed (Fig. 4, Supplementary table). For each cell population in each cluster, we identified specifically or highly expressed genes. Based on their embryonic stage and specifically known marker genes (Table 1 and Fig. 5), we manually annotated cell types to each of 15 clusters. Cluster 1 was mainly composed of E9.5 cells (Figs. 2, 3), indicating that this cluster contained a population of immature cells. As we describe below, we annotated the other 14 clusters

derived from five different embryonic stages as one of the four components of the inner ear: cochlea, vestibule, semicircular canal, and endolymphatic duct/sac, and further classified these clusters into sub-populations of these components. Accordingly, four clusters (clusters 6, 7, 8, and 9) were annotated as the cochlea, because these clusters were shown to highly express the known markers of sub-classified regions within the cochlea. Cluster 6, 7, and 9 contained E10.5–13.5 cells, while cluster 8 included E11.5–13.5 cells (Figs. 2, 3). This distribution indicated that clusters 6, 7, and 9 contained cells that were slightly more immature than those in cluster 8. Bone morphogenetic protein 4 (*Bmp4*) and GATA binding protein 3 (*Gata3*), which are known marker genes of the lateral (abneural) side of the cochlear duct floor, were expressed in cluster 7 at E12.5 and 13.5 (Table 1 and Fig. 6) (Luo et al., 2013; Ohyama et al., 2010), indicating that this cluster represented the lateral region of the cochlear floor. The tectorin alpha (*Tecta*), tectorin beta (*Tectb*), and fibroblast growth factor 10 (*Fgf10*), which are marker genes of the medial (neural) side of the cochlear duct floor, were observed to be expressed in cluster 8 (Table 1 and Figs. 5, 6) (Ohyama et al., 2010; Rau et al., 1999). By E13.5, SRY-box 2 (*Sox2*), which is necessary for the differentiation of sensory cells in the inner ear has been reported to become restricted to the prosensory domain (Kiernan et al., 2005). In our analysis, we detected that the expression of *Sox2* expression was less specific than expected at E13.5 (Fig. 5), and this result is consistent with a previous report (Gu et al., 2016), although it is possible that this was partly because of the shallow sequencing depth. Therefore, we annotated the prosensory domain of the cochlear duct using fibroblast growth factor 20 (*Fgf20*) expression (Table 1 and Fig. 5), which was reported to be specific to the prosensory region of the cochlear duct at E13.5 (Hayashi et al., 2008). All *Fgf20*-positive cells at E13.5 were included in

cluster 8, despite the fact that the prosensory domain of the cochlear duct did not form a distinct cluster. These expression patterns suggested that cluster 8 contained cell populations from the medial side and prosensory region of the cochlear floor. Cluster 9 was annotated as the cochlear roof because of its strong expression of orthodenticle homeobox 2 (*Otx2*) and orthodenticle homeobox 1 (*Otx1*), which are reported as cochlea roof markers at E10.5, 11.5, 12.5, and 13.5 (Table 1 and Fig. 5) (Morsli et al., 1999). Thyroid hormone receptor beta (*Thrb*) and clusterin (*Clu*), which are well known cochlea markers, were observed to be expressed in cluster 6 (Table 1 and Fig. 5). *Thrb* is known to be expressed in the ventro-medial portion of the otic vesicle, where the cochlea starts to extend (Bradley et al., 1994). Similarly, *Clu* is also known to be expressed in the ventro-medial portion of the otic vesicle (Lee et al., 2017). Therefore, considering the involvement of more E10.5 cell populations than those observed in cochlear clusters 7, 8, and 9 (Fig. 3), we assumed that cluster 6 might contain an otic vesicle cell population that would give rise to the cochlea. We annotated clusters 4 and 5, which contained E10.5–13.5 cells (Figs. 2, 3), as the vestibule. Cluster 4 was annotated as the macula (the vestibular prosensory/sensory region), because cells in the cluster were shown to express LFNG O-fucosylpeptide 3-beta-N-acetylglucosaminyltransferase (*Lfng*), neurotrophin 3 (*Ntf3*), and *Fgf10* that are known to be expressed in the macula and in the cochlear floor (Morsli et al., 1998; Pauley et al., 2003; Pirvola et al., 1992), whereas they did not express cochlear duct floor markers, such as *Clu* and *Thrb* (Table 1 and Fig. 5). The top 30 marker genes for cluster 4 included otogelin (*Otog*) and otogelin-like (*Otogl*), encoding otoconial membrane-forming proteins specific to the macula (Table 1 and Fig. 5) (Lundberg et al., 2015). In cluster 5, we observed the strong expression of paired box 2 (*Pax2*) and LIM

homeobox transcription factor 1 alpha (*Lmx1a*) (Table 1 and Fig. 5). In particular, *Pax2* has been shown to be most strongly expressed in the medial part of the otic vesicle at E10.5 and is known to be expressed in the non-sensory part of the vestibule at E13.5 (Liu et al., 2018). On the other hand, *Lmx1a* has been reported to be exclusively expressed in the non-sensory part of the inner ear at E13.5 (Fig. 5) (Koo et al., 2009). Cluster 5 did not express cochlear marker genes, such as *Clu* (Lee et al., 2017) and *Thrb* (Bradley et al., 1994), as well as sema domain, immunoglobulin domain (Ig), short basic domain, secreted, (semaphorin) 3E (*Sema3e*) (Miyazaki et al., 1999), a marker of the non-sensory part of the semicircular canal and the endolymphatic duct. Considering that cluster 5 did not express marker genes of the cochlear duct, semicircular canals, and the endolymphatic duct/sac, whereas expressed marker genes of the non-sensory part of the inner ear at E13.5, we annotated cluster 5 as the non-sensory domain of the vestibule. The clusters annotated as semicircular canals included clusters 10–15. Cluster 10 was mostly composed of E9.5–10.5 cells, whereas cluster 11–15 contained E10.5–13.5 cells (Figs 2, 3). All six clusters expressed otoconin 90 (*Oc90*) (Durruthy-Durruthy et al., 2015), a marker of the dorsal regions of the inner ear that give rise to the development of the semicircular canals and the endolymphatic duct (Table 1 and Fig. 5). We annotated cluster 15 as the crista (the semicircular canal sensory region), as it expressed *Bmp4*, which is a reported crista marker (Fig. 6) (Morsli et al., 1998). In contrast, clusters 11–14 were annotated as the non-sensory region of the semicircular canals because of the lack of *Bmp4* expression and their expression of *Sema3e*. It is known that *Sema3e* is a marker for the non-sensory part of the semicircular canals and the endolymphatic duct and is known to never be expressed in the cochlear duct (Table 1 and Fig. 5) (Miyazaki et al., 1999). To annotate cluster 10, composed of immature E9.5

and 10.5 cells, we used LIM domain only 4 (*Lmo4*), a marker reported to be expressed in the dorso-lateral part of the otocyst (Deng et al., 2006). This gene was strongly expressed in cluster 10 and thus, we annotated this cluster as an immature population of the semicircular canal, because the semicircular canal is known to originate from the dorso-lateral part of the otocyst (Li et al., 1978) and cluster 10 was located near the 11–14 semicircular canal clusters in UMAP plots. The clusters of endolymphatic duct/sac, including clusters 2 and 3, were defined by wingless-type MMTV integration site family, member 2B (*Wnt2b*), which is known to be an endolymphatic duct marker (Table 1 and Fig. 5) (Hatch et al., 2007). The endolymphatic duct and sac are known to originate from the dorso-medial part of otic vesicles (Brigande et al., 2000). Consistent with this, *Oc90* and *Pax2*, well-known dorsal and medial markers of otic vesicles, respectively, were observed to be expressed in cluster 2 and 3. At E10.5, dachshund family transcription factor 1 (*Dach1*) and dachshund family transcription factor 2 (*Dach2*), which are markers of the dorsal domain of the otic vesicle (Ayres et al., 2001; Miwa et al., 2019), were also shown to be expressed in both clusters (Table 1 and Fig. 5). Cluster 2 was composed of E9.5–10.5 cells, whereas cluster 3 was formed by E11.5–13.5 cells. Both clusters 2 and 3 were considered to be immature and mature cell populations of the endolymphatic duct/sac, respectively, based on their UMAP location.

3.2. Validation of the in silico analysis using in situ hybridisation (ISH)

To validate our in silico analysis of the scRNA-Seq data, we performed ISH experiments using cluster marker genes, whose expression was unknown in the inner ear at E9.5–13.5. First, we performed ISH on E13.5 inner ear horizontal sections (Fig. 7). Based on our in silico analysis, we selected a marker for each component within the

inner ear (Fig. 7A–D). Accordingly, our analysis predicted RAR related orphan receptor B (*Rorb*), zona pellucida like domain containing 1 (*Zpld1*), and E74-like factor 1 (*Elf1*) to be exclusively expressed in the cochlea duct floor, the crista, and the endolymphatic duct/sac, respectively. On the other hand, we predicted ADAMTS-like 1 (*Adamtsl1*) to be most enriched in the vestibular sensory region. Our ISH results revealed that the expression patterns for these four genes were consistent with our in silico analysis (Fig. 7). Recent studies suggested that *Rorb* and *Zpld1* were expressed in the developing cochlea (Li et al., 2020) and the newborn crista (Vijayakumar et al., 2019), respectively. In addition, we performed ISH for *Rorb* at various developmental stages (Fig. 8). Our ISH results confirmed its expression at the presumed cochlea floor, the ventro-medial part of the otocyst at E10.5 (Fig. 8A), and at the cochlea floor at E11.5 (Fig. 8B) and 12.5 (Fig. 8C), as well as at E13.5 (Fig. 8D). As another unknown gene specific to some clusters, we selected vav 3 oncogene (*Vav3*), which was one of the top 30 marker genes for cluster 5 (Supplementary table and Fig. 9 A–E). Cluster 5 was annotated as a non-sensory vestibule that was not well described in previous studies. Briefly, *Vav3* encodes a guanosine nucleotide exchange factor (GEF) that regulates Rho GTPases (Bustelo, 2014). Both GEF and Rho GTPases have been reported to exhibit critical functions in the development of the inner ear, where cytoskeletal organisation plays intriguing roles (Grimsley-Myers et al., 2012; Yamamoto et al., 2009). The UMAP plot for *Vav3* revealed its strong expression in cluster 5 (circle in Fig. 9A), and its moderate expression in clusters 2 and 3 (dotted circle in Fig. 9A). Our ISH results (Fig. 9B, D, and E) showed that *Vav3* was expressed in the non-sensory part of the vestibule (NSV in Fig. 9B and D) and the endolymphatic duct (ED in Fig. 9 B and E) at E13.5, as predicted in our silico analysis, as well as in the spiral ganglion (SG in Fig. 9B) and

vestibular ganglion (VG in Fig. 9D). We also used *Sox2* as a marker of the vestibular prosensory part (Fig 9C).

3.3 Analysis of differentially expressed genes of the cochlea and the vestibule clusters

To identify genes specific to the regions determined to develop into the cochlear or vestibular sensory organs at E10.5, we compared the transcriptome of the cochlea floor (clusters 6 and 7) with that of the prosensory region of the vestibule (cluster 4). Table 2 shows the list of upregulated differentially expressed genes (DEGs) in the cochlear duct floor and the prosensory part of the vestibule. The cochlea duct floor cluster were shown to have nine upregulated DEGs, including five transcription factors (GO:0006351~transcription, DNA-templated) [*Rorb*, *Pax2*, *Dach1*, nuclear receptor subfamily 2, group F, member 1 (*Nr2f1*), and PR domain containing 16 (*Prdm16*)], while the vestibule prosensory region cluster had 14 upregulated DEGs, including four transcription factors [neuronal PAS domain protein 3 (*Npas3*), erb-b2 receptor tyrosine kinase 4 (*Erbb4*), zinc finger protein 536 (*Zfp536*), and early B cell factor 3 (*Ebf3*)]. As we showed, one of these genes, *Rorb*, was observed to be exclusively expressed in the cochlear duct and not in the vestibule.

We explored genes common to the prosensory/sensory region by comparing the transcriptomes of clusters 4, 8, and 15, which contain sensory/prosensory cells of the macula, cochlear, and crista, respectively, with those of the rest, except for cluster 1. We detected 24 upregulated genes in the prosensory region [neurexin III (*Nrxn3*), early B cell factor 1 (*Ebf1*), *Adamtsl1*, phosphodiesterase 4B, cAMP specific (*Pde4b*), catenin (cadherin associated protein), alpha 2 (*Ctnna2*), sorbin and SH3 domain containing 2

(*Sorbs2*), transforming growth factor beta 2 (*Tgfb2*), transient receptor potential cation channel, subfamily M, member 3 (*Trpm3*), EYA transcriptional coactivator and phosphatase 4 (*Eya4*), *Fgf10*, SH3-domain GRB2-like 2 (*Sh3gl2*), *Npas3*, roundabout guidance receptor 1 (*Robo1*), *Ntf3*, *Zfp536*, carbohydrate (N-acetylgalactosamine 4-0) sulfotransferase 9 (*Chst9*), thymocyte selection-associated high mobility group box (*Tox*), sparc/osteonectin, cwcv and kazal-like domains proteoglycan 1 (*Spock1*), EYA transcriptional coactivator and phosphatase 1 (*Eya1*), sidekick cell adhesion molecule 1 (*Sdk1*), NHS actin remodeling regulator (*Nhs*), teneurin transmembrane protein 4 (*Tenm4*), autism susceptibility candidate 2 (*Auts2*), and formin 1 (*Fmn1*)]. Among these genes, we examined the expression of *Ebf1* (Liberg et al., 2002) (Fig. 9 F–K), one of the basic helix loop helix (bHLH) transcription factors, because many kinds of bHLH transcriptional factors, including atonal bHLH transcription factor 1 (*Atoh1*), hes family bHLH transcription factor 1 (*Hes1*), and hes family bHLH transcription factor 5 (*Hes5*), are known to be involved in the development of the sensory region within the inner ear (Zine et al., 2001). Our ISH analysis (Fig. 9G, I, and K) revealed that *Ebf1* was expressed in the medial side of the cochlear duct, including the prosensory region (CD in Fig. 9G, I and K), the macular prosensory region (SM in Fig. 9I), the crista (PC in Fig. 9K), and the spiral ganglion (SG in Fig. 9I) at E13.5. Accordingly, we adopted *Sox2* as a marker of the prosensory region of the cochlear duct, vestibule, and semicircular canal (Fig. 9H and J).

4. **Discussion**

To obtain a global view of the early development of the inner ear, in this study, we analysed the transcriptomes of 5,000 otic epithelial cells from mouse embryos spanning

E9.5 to E13.5, downloaded from the Mouse Organogenesis Cell Atlas (Cao et al., 2019). Cao et al. profiled the transcriptomes of 2,000,000 whole-body embryo cells and identified 10 main trajectories, one of which was epithelial trajectory. Applying Louvain clustering for the epithelial trajectory, they identified 10 sub-trajectories such as apical ectodermal ridge and auditory epithelial trajectories. The auditory epithelial trajectory was composed of three populations, namely otic vesicle epithelium, otic sensory epithelium, and utricle and saccule epithelium (Cao et al., 2019). Although they analysed the apical ectodermal ridge trajectory in detail, their annotation was preliminary for the other trajectories. Because three clusters are not considered to be sufficient to explain the heterogeneity of the otic epithelial cells, we performed more detailed analyses on the data from the auditory epithelial trajectory. This is the first study analysing the otocyst at serial developmental stages at single-cell resolution and at the transcriptome level. In our analysis, we visualised that the otic epithelial progenitors differentiated into four inner ear components and subtypes of each tissue through embryonic stages from E9.5 to E13.5 (Figs. 2, 3), and we subsequently identified new candidate marker genes for each cell population. Although the auditory epithelial trajectory was defined by four markers, the gene expression patterns of 5000 cells in the dataset were mostly consistent with those of otic cells. Of course, very immature otic epithelial cells whose markers are unknown may not be involved in the current analysis.

Most of the E9.5 otic epithelial cells were observed to be contained in cluster 1, with a part of E9.5 cells forming cluster 10 (the semicircular canal) and cluster 2 (the endolymphatic duct/sac). Cluster 4 (the macula), cluster 5 (the non-sensory part of the vestibule), and cluster 6, which presumably indicated the cell population giving rise to the cochlea, were shown to contain E10.5 cells (Figs. 2, 3). Likewise, E10.5 cells were

found in clusters annotated as comparatively more matured cell populations, including cluster 7 (the lateral side of the cochlea duct floor), cluster 9 (the cochlea roof), cluster 15 (the crista), and cluster 10–14 (the non-sensory part of the semicircular canals). These results collectively suggested that differentiation toward the four components of the inner ear begins at E9.5 or E10.5. In addition, we noted that cluster 8 (expressing the markers for the medial side of the cochlear duct floor) appeared at E11.5, suggesting that the formation of the medial-lateral axis of the cochlear duct floor start at this stage. This observation was consistent with previous reports regarding the formation of the medial-lateral axis within the cochlear duct. Both *Bmp4* (Ohyama et al., 2010) and *Fgf10* (Urness et al., 2015) were observed to be expressed in the lateral and medial side of the cochlear duct from E11.5, respectively. Likewise, our in silico analysis also detected the expression of *Bmp4* and *Fgf10* in the clusters 7 and 8, respectively, at E11.5 (Fig. 6).

The apical-basal axis, the other axis of the cochlear turn, is known to be relevant to a functional role called tonotopy. One of genes considered to be involved in the formation of this axis is follistatin (*Fst*) (Son et al., 2012), which is reported to show higher expression in the apical turn of the developing cochlea. The UMAP plot showed that the expression of the *Fst* gene, which was expected to be more in the apical turn of the cochlea, was restricted to cluster 7 (Fig. 5). This expression pattern was consistent with a previous report showing that *Fst* was expressed in the lateral side of the cochlear duct floor (Son et al., 2012), and hence we assumed that cluster 7 might contain the apical cochlear duct cells. However, no apparent clusters representing the apical or basal turn of the cochlear were identified, and as such, we could not discriminate the cochlear duct floor cells of the apical turn from those of the basal turn in our dataset even after

re-clustering the cochlear floor clusters (clusters 6, 7, and 8). This might have been due to the gradual difference in the gene expression along the apical-basal axis.

The identification of candidates of cell sub-populations enabled us to compare the transcriptomes between specific cell sub-populations. For example, we compared the transcriptome of the cochlear duct floor with that of a vestibular prosensory region. Regarding the comparison between cells of the cochlea and the vestibular organs, Scheffer et al. have previously investigated the difference between the cochlear and the vestibular hair cells at the transcriptome level at E16, P0, P4, and P7 (Scheffer et al., 2015). Similarly, Burns et al. investigated the transcriptome of hair cells, supporting cells in the cochlea and the vestibule of P1 mice at the single-cell level (Burns et al., 2015). However, a comparison of the transcriptome of the cochlear duct floor and that of the vestibular prosensory region at an earlier developmental stage has not been made. The identified transcriptomic differences between the cochlea and the vestibule during the early development will help us clarify the mechanism of cell fate decision in the inner ear at this stage. We detected 23 DEGs between the cochlea and the vestibule (Table 2). We focused on *Rorb*, because it was exclusively found in the cochlea and never detected in the semicircular canals, endolymphatic duct/cyst or the vestibule in our in silico analysis. We observed that *Rorb* was only expressed in the presumed cochlear duct at E10.5 (Fig. 8A), suggesting that other DEGs predicted to be only expressed in the cochlear or vestibule in our in silico analysis might be important for the fate decision within the inner ear in this comparison.

Although an in silico analysis using public data might be powerful and promising in identifying intriguing genes during the developmental stages, as shown in this study (Figs. 7–9), this approach had limitations. First, the sequencing depth of the dataset was

shallow and the median UMIs and detected genes per cell for the 5,000 cells we analysed were just 805 and 614, respectively (see the Materials and Methods section). Heimberg et al. (Heimberg et al., 2016) evaluated the impact of the sequencing depth using the data of Zeisel et al. (Zeisel et al., 2015), in which they captured ~15,000 UMIs for each cell in a single-cell analysis of the brain. Although Heimberg et al. reported that 1,000 UMIs were enough to detect several cell types (Heimberg et al., 2016), and we did identify many cell populations, we might have still missed some cell populations. As a matter of fact, we could not discriminate between the hair cells from the supporting cells in cluster 4 in our analysis, even though the first differentiating hair cells in the vestibule macula could be seen by E12 (Raft et al., 2007). With deeper sequencing data, we might achieve a finer sub-classification of the inner ear based on transcriptomic analysis. Nonetheless, despite its shallow sequencing depth, our study discovered several new marker genes, suggesting that the scRNA-seq approach could be useful in studies of the development of the inner ear.

Second, our dataset only included the epithelial cells and not the neuroblasts that constitute the developing inner ear. We expected to specify an otic neuroblast cluster, originating in the ventro-anterior region of the otic vesicle, where they are known to delaminate and migrate to form the cochleo-vestibular ganglion; however, we did not discover any cell population expressing neuroblast marker genes, such as neurogenin 1 (*Neurog1*), and neuronal differentiation 1 (*Neurod1*) (Liu et al., 2000; Ma et al., 1998). To determine the development of the whole inner ear, we should have additionally analysed several neuro-trajectories in the Mouse Organogenesis Cell Atlas, which might have contained the otic neuroblasts.

Conclusion

We visualised a transcriptome of 5,000 cells and suggested the means by which E9.5 otic epithelial cells differentiate into the cochlea, the vestibule, the semicircular canals, and the endolymphatic duct/sac based on our analysis of single-cell gene expression. We also identified candidates of new marker genes defining sub-populations of the four components of the inner ear. These results will help further studies on inner ear development.

Acknowledgements

DNA sequencing analysis was performed at the Medical Research Support Center, Graduate School of Medicine, Kyoto University.

Declaration of competing interests

The authors declare that they have no competing interests.

Author contributions

RY performed the in silico analysis. RY and HO performed all in vivo experiments, RY and NY wrote the manuscript. KO contributed to the revision of the manuscript. All authors discussed the results and contributed to the final manuscript. NY conceived the presented study and supervised the whole project.

Funding

This work was supported by the Project for JSPS KAKENHI (Grant number 19H03803) to NY. The sponsors of this study had no role in the study design, data analysis, or data interpretation or the writing of the report.

Data availability

The single-cell transcriptome dataset we analysed can be downloaded from Mouse Organogenesis Cell Atlas (https://oncoscape.v3.sttrcancer.org/atlas.gs.washington.edu.mouse.rna/downloads) (Cao et al., 2019).

The raw and processed data can be downloaded from the NCBI Gene Expression Omnibus under accession number GSE119945.

References

Ayres, J.A., Shum, L., Akarsu, A.N., Dashner, R., Takahashi, K., Ikura, T., Slavkin, H.C., Nuckolls, G.H., 2001. DACH: genomic characterization, evaluation as a candidate for postaxial polydactyly type A2, and developmental expression pattern of the mouse homologue. Genomics 77, 18-26.

Bradley, D.J., Towle, H.C., Young, W.S., 1994. α And ß thyroid hormone receptor (TR) gene expression during auditory neurogenesis: Evidence for TR isoform-specific transcriptional regulation in vivo. Proceedings of the National Academy of Sciences of the United States of America 91, 439-443.

Brigande, J.V., Iten, L.E., Fekete, D.M., 2000. A fate map of chick otic cup closure reveals lineage boundaries in the dorsal otocyst. Developmental Biology 227, 256-270.

Burns, J.C., Kelly, M.C., Hoa, M., Morell, R.J., Kelley, M.W., 2015. Single-cell RNA-Seq resolves cellular complexity in sensory organs from the neonatal inner ear. Nature Communications 6, 1-16.

Bustelo, X.R., 2014. Vav family exchange factors: an integrated regulatory and functional view. Small GTPases 5, 9.

Cao, J., Spielmann, M., Qiu, X., Huang, X., Ibrahim, D.M., Hill, A.J., Zhang, F., Mundlos, S., Christiansen, L., Steemers, F.J., Trapnell, C., Shendure, J., 2019. The single-cell transcriptional landscape of mammalian organogenesis. Nature 566, 496-502.

Deng, M., Pan, L., Xie, X., Gan, L., 2006. Differential expression of LIM domain-only (LMO) genes in the developing mouse inner ear. Gene Expression Patterns 6, 857-863.

Durruthy-Durrthy, R., Gottlieb, A., Hartman, B.H., Waldhaus, J., Laske, R.D., Altman, R., Heller, S., 2014. Reconstruction of the mouse otocyst and early neuroblast lineage at single cell resolution. Cell 157, 964-978.

Durruthy-Durruthy, R., Hartman, B.H., Losorelli, S., Laske, R.D., Heller, S., 2015. Identification and characterization of mouse otic sensory lineage genes. Frontiers in Cellular Neuroscience 9, 79.

Grimsley-Myers, C.M., Sipe, C.W., Wu, D.K., Lu, X., 2012. Redundant functions of Rac GTPases in inner ear morphogenesis. Developmental Biology 362, 172-186.

Gu, R., Brown, R.M., Hsu, C.W., Cai, T., Crowder, A.L., Piazza, V.G., Vadakkan, T.J., Dickinson, M.E., Groves, A.K., 2016. Lineage tracing of Sox2-expressing progenitor cells in the mouse inner ear reveals a broad contribution to non-sensory tissues and insights into the origin of the organ of Corti. Developmental Biology 414, 72-84.

Hafemeister, C., Satija, R., 2019. Normalization and variance stabilization of single-cell RNA-seq data using regularized negative binomial regression. Genome Biology 20, 296.

Hatch, E.P., Noyes, C.A., Wang, X., Wright, T.J., Mansour, S.L., 2007. Fgf3 is required for

dorsal patterning and morphogenesis of the inner ear epithelium. Development 134, 3615-3625.
Hayashi, T., Ray, C.A., Bermingham-McDonogh, O., 2008. Fgf20 is required for sensory epithelial specification in the developing cochlea. Journal of Neuroscience 28, 5991-5999.
Heimberg, G., Bhatnagar, R., El-Samad, H., Thomson, M., 2016. Low dimensionality in gene expression data enables the accurate extraction of transcriptional programs from shallow sequencing. Cell Systems 2, 239-250.
Hoffman, P., Satija, R., Papalexi, E., Smibert, P., Butler, A., 2018. Integrating single-cell transcriptomic data across different conditions, technologies, and species. Nature Biotechnology 36, 411-420.
Kiernan, A.E., Pelling, A.L., Leung, K.K.H., Tang, A.S.P., Bell, D.M., Tease, C., Lovell-Badge, R., Steel, K.P., Cheah, K.S.E., 2005. Sox2 is required for sensory organ development in the mammalian inner ear. Nature 434, 1031-1035.
Koo, S.K., Hill, J.K., Hwang, C.H., Lin, Z., Millen, K.J., Wu, D.K., 2009. Lmx1a maintains proper neurogenic, sensory, and nonsensory domains in the mammalian inner ear. Developmental Biology 333, 14-25.
La Manno, G., Soldatov, R., Zeisel, A., Braun, E., Hochgerner, H., Petukhov, V., Lidschreiber, K., Kastriti, M.E., Lönnerberg, P., Furlan, A., Fan, J., Borm, L.E., Liu, Z., Van Bruggen, D., Guo, J., He, X., Barker, R., Sundström, E., Castelo-Branco, G., Cramer, P., Adameyko, I., Linnarsson, S., Kharchenko, P.V., 2018. RNA velocity of single cells. Nature 560, 494-498.
Lee, S., Shin, J.O., Sagong, B., Kim, U.K., Bok, J., 2017. Spatiotemporal expression patterns of clusterin in the mouse inner ear. Cell and Tissue Research 370, 89-97.
Li, C., Wang, Y., Wang, G., Lu, Y., He, S., Sun, Y., Liu, Z., 2020. Fate-mapping analysis using Rorb-IRES-Cre reveals apical-to-basal gradient of Rorb expression in mouse cochlea. Developmental Dynamics 249, 173-186.
Li, C.W., Van De Water, T.R., Ruben, R.J., 1978. The fate mapping of the eleventh and twelfth day mouse otocyst: an in vitro study of the sites of origin of the embryonic inner ear sensory structures. Journal of Morphology 157, 249-267.
Liberg, D., Sigvardsson, M., Akerblad, P., 2002. The EBF/Olf/Collier family of transcription factors: regulators of differentiation in cells originating from all three embryonal germ layers. Molecular and Cellular Biology 22, 8389-8397.
Liu, M., Pereira, F.A., Price, S.D., Chu, M.J., Shope, C., Himes, D., Eatock, R.A., Brownell, W.E., Lysakowski, A., Tsai, M.J., 2000. Essential role of BETA2/NeuroD1 in development of the vestibular and auditory systems. Genes and Development 14, 2839-2854.
Liu, S., Wang, Y., Lu, Y., Li, W., Liu, W., Ma, J., Sun, F., Li, M., Chen, Z.-Y., Su, K., Li, W., 2018. The key transcription factor expression in the developing vestibular and auditory

sensory organs: a comprehensive comparison of spatial and temporal patterns. Neural Plasticity 2018, 1-9.
Lundberg, Y.W., Xu, Y., Thiessen, K.D., Kramer, K.L., 2015. Mechanisms of otoconia and otolith development. Developmental Dynamics 244, 239-253.
Luo, X.j., Deng, M., Xie, X., Huang, L., Wang, H., Jiang, L., Liang, G., Hu, F., Tieu, R., Chen, R., Gan, L., 2013. GATA3 controls the specification of prosensory domain and neuronal survival in the mouse cochlea. Human Molecular Genetics 22, 3609-3623.
Ma, Q., Chen, Z., Barrantes, I.D.B., De La Pompa, J.L., Anderson, D.J., 1998. Neurogenin1 is essential for the determination of neuronal precursors for proximal cranial sensory ganglia. Neuron 20, 469-482.
McInnes, L., Healy, J., Melville, J., 2018. UMAP: Uniform Manifold Approximation and Projection for Dimension Reduction. arXiv:1802.03426v2.
Miwa, T., Minoda, R., Ishikawa, Y., Kajii, T., Orita, Y., Ohyama, T., 2019. Role of Dach1 revealed using a novel inner ear-specific Dach1-knockdown mouse model. Biology Open 8, bio043612.
Miyazaki, N., Furuyama, T., Takeda, N., Inoue, T., 1999. Expression of mouse semaphorin H mRNA in the inner ear of mouse fetuses. Neuroscience Letters 261, 127-129.
Morsli, H., Choo, D., Ryan, A., Johnson, R., Wu, D.K., 1998. Development of the mouse inner ear and origin of its sensory organs. Journal of Neuroscience 18, 3327-3335.
Morsli, H., Tuorto, F., Choo, D., Postiglione, M.P., Simeone, A., Wu, D.K., 1999. Otx1 and Otx2 activities are required for the normal development of the mouse inner ear. Development 126, 2335-2343.
Ohnishi, H., Skerleva, D., Kitajiri, S., Sakamoto, T., Yamamoto, N., Ito, J., Nakagawa, T., 2015. Limited hair cell induction from human induced pluripotent stem cells using a simple stepwise method. Neuroscience Letters 599, 49-54.
Ohyama, T., Basch, M.L., Mishina, Y., Lyons, K.M., Segil, N., Groves, A.K., 2010. BMP signaling is necessary for patterning the sensory and nonsensory regions of the developing mammalian cochlea. Journal of Neuroscience 30, 15044-15051.
Oshima, K., Shin, K., Diensthuber, M., Peng, A.W., Ricci, A.J., Heller, S., 2010. Mechanosensitive hair cell-like cells from embryonic and induced pluripotent stem cells. Cell 141, 704-716.
Pauley, S., Wright, T.J., Pirvola, U., Ornitz, D., Beisel, K., Fritzsch, B., 2003. Expression and function of FGF10 in mammalian inner ear development. Developmental Dynamics 227, 203-215.
Pirvola, U., Ylikoski, J., Palgi, J., Lehtonen, E., Arumae, U., Saarma, M., 1992. Brain-derived neurotrophic factor and neurotrophin 3 mRNAs in the peripheral target fields

of developing inner ear ganglia. . Proceedings of the National Academy of Sciences of the United States of America 89, 9915-9919.
Raft, S., Koundakjian, E.J., Quinones, H., Jayasena, C.S., Goodrich, L.V., Johnson, J.E., Segil, N., Groves, A.K., 2007. Cross-regulation of Ngn1 and Math1 coordinates the production of neurons and sensory hair cells during inner ear development. Development 134, 4405-4415.
Rau, A., Legan, K.P., Richardson, G.P., 1999. Tectorin mRNA expression is spatially and temporally restricted during mouse inner ear development. Journal of Comparative Neurology 405, 271-280.
Sai, X., Ladher, R.K., 2015. Early steps in inner ear development: Induction and morphogenesis of the otic placode. Frontiers in Pharmacology 6, 1-8.
Scheffer, D.I., Shen, J., Corey, D.P., Chen, Z.Y., 2015. Gene expression by mouse inner ear hair cells during development. Journal of Neuroscience 35, 6366-6380.
Shapiro, E., Biezuner, T., Linnarsson, S., 2013. Single-cell sequencing-based technologies will revolutionize whole-organism science. Nature Reviews Genetics 14, 618-630.
Son, E.J., Wu, L., Yoon, H., Kim, S., Choi, J.Y., Bok, J., 2012. Developmental gene expression profiling along the tonotopic axis of the mouse cochlea. PLoS One 7, e40735.
Stuart, T., Butler, A., Hoffman, P., Hafemeister, C., Papalexi, E., Mauck, W.M., Hao, Y., Stoeckius, M., Smibert, P., Satija, R., 2019. Comprehensive integration of single-cell data. Cell 177, 1888-1902.e1821.
Treutlein, B., Brownfield, D.G., Wu, A.R., Neff, N.F., Mantalas, G.L., Espinoza, F.H., Desai, T.J., Krasnow, M.A., Quake, S.R., 2014. Reconstructing lineage hierarchies of the distal lung epithelium using single-cell RNA-seq. Nature 509, 371-375.
Urness, L.D., Wang, X., Shibata, S., Ohyama, T., Mansour, S.L., 2015. Fgf10 is required for specification of non-sensory regions of the cochlear epithelium. Developmental Biology 400, 59-71.
Vijayakumar, S., Jones, S.M., Jones, T.A., Tian, C., Johnson, K.R., 2019. Spontaneous mutations of the Zpld1 gene in mice cause semicircular canal dysfunction but do not impair gravity receptor or hearing functions. Scientific Reports 9, 1-15.
Wolock, S.L., Lopez, R., Klein, A.M., 2019. Scrublet: Computational Identification of Cell Doublets in Single-Cell Transcriptomic Data. Cell Systems 8, 281-291.e289.
Yamamoto, N., Okano, T., Ma, X., Adelstein, R.S., Kelley, M.W., 2009. Myosin II regulates extension, growth and patterning in the mammalian cochlear duct. Development 136, 1977-1986.
Zeisel, A., Munoz-Manchado, A.B., Codeluppi, S., Lonnerberg, P., La Manno, G., Jureus, A., Marques, S., Munguba, H., He, L., Betsholtz, C., Rolny, C., Castelo-Branco, G.,

Hjerling-Leffler, J., Linnarsson, S., 2015. Brain structure. Cell types in the mouse cortex and hippocampus revealed by single-cell RNA-seq. Science 347, 1138-1142.
Zine, A., Aubert, A., Qiu, J., Therianos, S., Guillemot, F., Kageyama, R., de Ribaupierre, F., 2001. Hes1 and Hes5 activities are required for the normal development of the hair cells in the mammalian inner ear. The Journal of Neuroscience 21, 4712-4720.

Figure legends

Fig. 1. **Scheme of the development of the inner ear.**

The four anatomical structures in the inner ear remain morphologically undefined at embryonic day 10.5 (E10.5), becoming clearer at E13.5. The cochlear duct (CD) and the vestibule (Ves) are derived from the ventral half and the ventral-to-middle part of the otic vesicle (E10.5), respectively. The endolymphatic duct/sac (ED) and the semicircular canal (SC), arise from the dorso-medial and dorso-lateral parts of the otic vesicle, respectively. These four structures are clearly segregated at E12–13. A: anterior; D: dorsal; L: lateral.

Fig. 2. **UMAP plots coloured by clusters.**

We visualised the transcriptional states of 5,000 cells using UMAP. Each point indicates one of the 5,000 cells. Applying the Louvain clustering algorithm for community detection, we identified 15 clusters. Clusters were annotated based on established marker genes (Table 1). We annotated clusters 2 and 3 as the endolymphatic duct (ED), 4 and 5 as the vestibule (Ves), 6–9 as the cochlear duct (CD), and 10–15 as the semicircular canal (SC). Refer to the main text for the sub-classified annotation of each cluster. Lat: lateral side of the cochlear duct floor; Med: medial side of the cochlear duct floor. Roof: roof of the cochlear duct.

Fig. 3. **UMAP 2D-visualisation separated by developmental stages.**

We separated the Fig. 2 according to developmental stages (E9.5–13.5). E9.5 cells are located at the centre of the plot. With the proceeding of the developmental stages, each cell is shown to be distributed from the centre to the periphery.

Fig. 4. **Heatmap plot of cells by gene expression.**

Heatmap plot showing the expression levels of the top 30 marker genes of each cluster (y-axis) for 5,000 cells (x-axis). The genes are sorted in the order of the larger fold change of the mean expression value that was compared between the cluster and the other clusters. Marker genes common to more than one cluster are shown only once. Yellow indicates high gene expression, whereas magenta indicates low gene expression. CD: cochlear duct; ED: endolymphatic duct/sac; SC: semicircular canal; Ves: vestibule.

Fig. 5. **UMAP plot for marker genes.**

The expression level of known marker genes was plotted on an UMAP plot of all 5,000 cells. Each gene is a marker of some cell populations in the early developing inner ear. Plots are arranged in the alphabetical order.

Fig. 6. **UMAP plot for *Bmp4*, *Gata3*, and *Fgf10* at E11.5, 12.5, and 13.5.**

UMAP plot showing the expression patterns of *Bmp4*, *Gata3*, and *Fgf10* at different embryonic stages. These genes were used to define clusters 7 and 8.

Fig. 7. **UMAP plot of selected marker genes and in situ hybridisation (ISH) for these genes at E13.5.**

UMAP plots for four selected genes (A–D). Low-magnification fields of ISH images (E–H), and high-magnification fields of ISH images (I–T), of the inner ear at E13.5. Our ISH analysis showed that the mRNA expression pattern was in accordance with our in silico analysis. Accordingly, *Rorb* (A, E, I, M, and Q), *Zpld1*(C, G, K, O, and S), and *Elf1* (D, H, L, P, and T) are expressed only in the cochlea (CD in E and I), the crista (Cri in G and O), and the endolymphatic duct (ED in H and T), respectively. Likewise, *Adamtsl1* (B, F, J, N, and R) is expressed in the macula (UM and SM in F and J) and the nonsensory part of the semicircular canal (NSC in N and R) at E13.5 with its expression being most enriched in the macula, as predicted by our in silico analysis. CD: cochlear duct, Cri: Crista, ED: endolymphatic duct, NSC: nonsensory part of the semicircular canal, SC: semicircular canal, SM: saccular macul, Ves: vestibule, UM: utricular maculaa. D: dorsal; M: medial. Scale bars indicate 500 (E–H) and 200 (I–T) μm.

Fig. 8. **In situ hybridisation (ISH) for *Rorb* on the transverse inner ear section at E10.5–13.5.**

Our ISH analysis showed the expression of *Rorb* exclusively limited in the presumed cochlear duct at E10.5 (PCD in A) and the cochlear duct floor at E11.5 (B), 12.5 (C), and 13.5 (D) (CD in B, C, and D). CD: cochlear duct, PCD: presumed cochlear duct, Ves: vestibule. D: dorsal; M: medial. Scale bars indicate 200 μm.

Fig. 9. **Expression patterns of *Vav3* and *Ebf1*.**

The UMAP plot of *Vav3* (A) and *Ebf1* (F) and in situ hybridisation (ISH) for *Sox2* (C, H and J), *Vav3* [(B (Low-magnification field); D and E (High-magnification field)], and *Ebf1* [(G (Low-magnification field); I and K (High-magnification field)] at E13.5.

Adjacent sections were used for ISH of *Sox2* and *Vav3* (C and D, respectively) and *Sox2* and *Ebf1* (H and I, and J and K, respectively). Briefly, *Sox2* is expressed in the prosensory part of the cochlear duct (CD in H and J), the vestibule (UM and SM in C; SM in H), and the semicircular canal (LC in C; PC in J), and weakly in the vestibular and spiral ganglion cells (VG in C and SG in H, respectively). Accordingly, our in silico analysis showed that *Vav3* is most strongly expressed in cluster 5 (circled region indicating the non-sensory part of the vestibule in A) and in clusters 2 and 3 (dotted circle region indicating endolymphatic duct/sac in A). Our ISH results showed that *Vav3* is expressed in the non-sensory part of the vestibule (NSV in B and D) and in the endolymphatic duct (ED in B and E), as predicted by our in silico analysis, as well as in the spiral and vestibular ganglion (SG in B and VG in D, respectively). Our in silico analysis showed that *Ebf1* is expressed in the medial (neural) side of the cochlear duct (circled region in F), the sensory part of the vestibule (dotted circle region in F), and that of the crista (grey circle in F). Respectively, ISH revealed that *Ebf1* is expressed in the cochlear prosensory epithelia (CD in I and K) as well as in spiral ganglion cells (SG in I), and weakly in the macula (SM in I) and the crista (PC in K), as predicted by our in silico analysis. CD in B, G, H, I, J and K: cochlear duct, ED in B and E: endolymphatic duct, LC in C and D: lateral crista, NSV in B and D: non-sensory part of the vestibule, PC in J and K: posterior crista, SG in B, H and I: spiral ganglion, Ves in B and G: vestibule, UM in C and D: utricular macula, SC in G: semicircular canal, SM in C, D, H and I: saccular macula, VG in C and D: vestibular ganglion. D: dorsal, M: medial. Scale bars indicate 500 (B and G) and 200 (C–E and H–K) μm.

Tables

Table 1

E10.5

Ventral			Dorsal			Medial
VM	**VL**	**Whole Ventral**	**DM**	**DL**	**Whole Dorsal**	**Whole Medial**
Clu	*Oc90*	*Otol1*	*Wnt2b*	*Bmp4*	*Bmper*	*Pax2*
Fgf10	*Otx1*	*Six1*		*Lmo4*	*Dach1*	
Jag1	*Otx2*	*Eya1*			*Dach2*	
Lfng		*Eya4*			*Oc90*	
Ntf3						
Thrb						

E13.5

Cochlea				Vestibule		SC		ED
Medial side	**Prosensory**	**Lateral side**	**Roof**	**Macula**	**Vestibule non-sensory**	**Crista**	**SC non-sensory**	**ED**
Tecta	*Fgf20*	*Bmp4*	*Otx1*	*Lfng*	*Pax2*	*Bmp4*	*Seme3e*	*Dach1*
Tectb	*Ntf3*	*Emx2*	*Otx2*	*Fgf10*	*Lmx1a*	*Lmo4*	*Oc90*	*Dach2*
Fgf10	*Jag1*	*Gata3*	*Fgf9*	*Ntf3*		*Oc90*		*Lmx1a*
Jag1	*Hey2*	*Clu*	*Oc90*	*Tecta*				*Oc90*
	Isl1	*Fst*		*Otog*				*Sema3e*
		Isl1		*Otogl*				*Wnt2b*

Table 1. **Lists of E10.5 and 13.5 inner ear marker genes used in annotating the clusters.** DM: dorso-medial, DL: dorso-lateral, ED: endolymphatic duct, SC: semicircular canal, VL: ventro-lateral, VM: ventro-medial.

Table 2

Up DEGs in the cochlear duct	Up DEGs in the vestibular sensory part

Gene	Avg logFC	Adj p value	Gene	Avg logFC	Adj p value
Sulf1	1.052	5.03E-14	*Adamtsl1*	1.376	5.47E-20
Rorb	0.860	6.03E-09	*Pde4b*	0.925	1.81E-09
Pax2	0.704	1.14E-05	*Ccser1*	0.880	3.00E-12
Gpc5	0.613	1.27E-02	*Npas3*	0.755	1.12E-03
Dach1	0.539	2.03E-02	*Erbb4*	0.728	1.52E-08
Trappc9	0.383	3.20E-02	*Efna5*	0.544	2.06E-02
Nr2f1	0.381	2.78E-03	*Ctnna2*	0.529	1.80E-02
Itih5	0.362	6.60E-04	*Sh3gl2*	0.488	1.03E-05
Prdm16	0.362	2.69E-02	*Zfp536*	0.473	3.13E-04
			Ntf3	0.467	9.63E-03
			Ptprt	0.424	2.88E-04
			Ebf3	0.398	1.44E-03
			Plxna4	0.346	4.44E-02
			Gas1	0.325	7.13E-04

Table 2. Differentially expressed genes in the cochlear duct floor and the prosensory part of the vestibule sorted in the order of the larger fold change. We applied differential expression analysis using Wilcoxon rank-sum test for the cochlear duct floor cells and the prosensory part of the vestibule at E10.5. Adj p value: p value adjusted by Bonferroni correction, Avg logFC: average log fold change, Up DEGs: upregulated differentially expressed genes.

Main text: 5520 words, Figure legends: 1061 words (less than 7,000 words)

Fig. 1

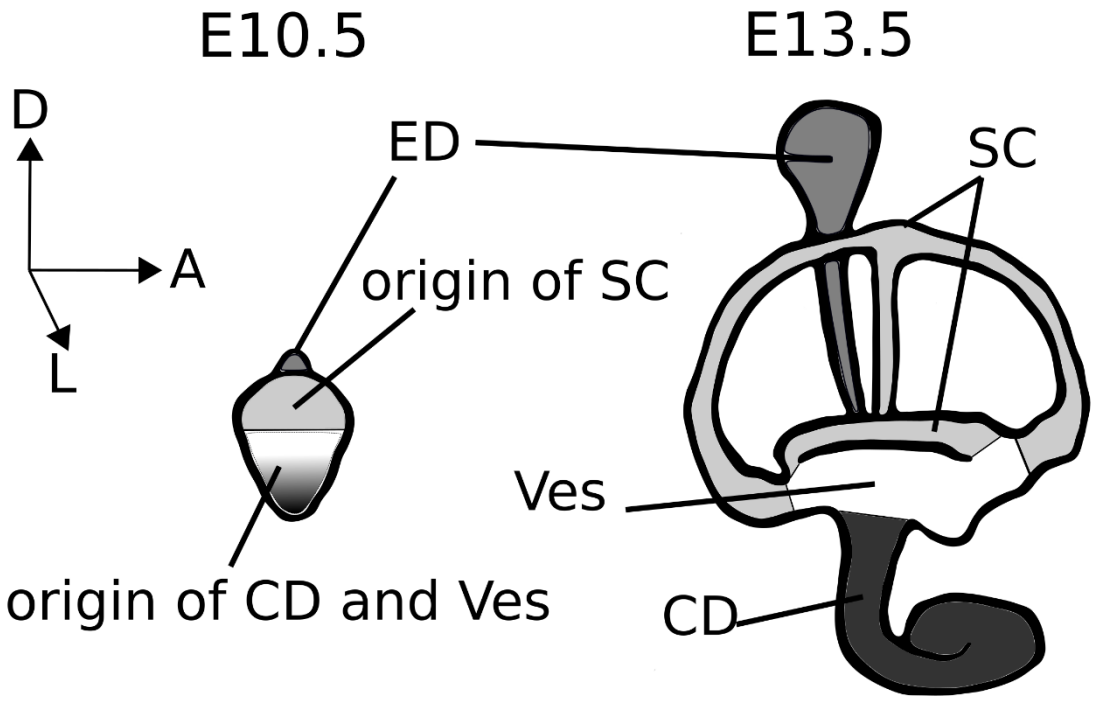

Fig. 2

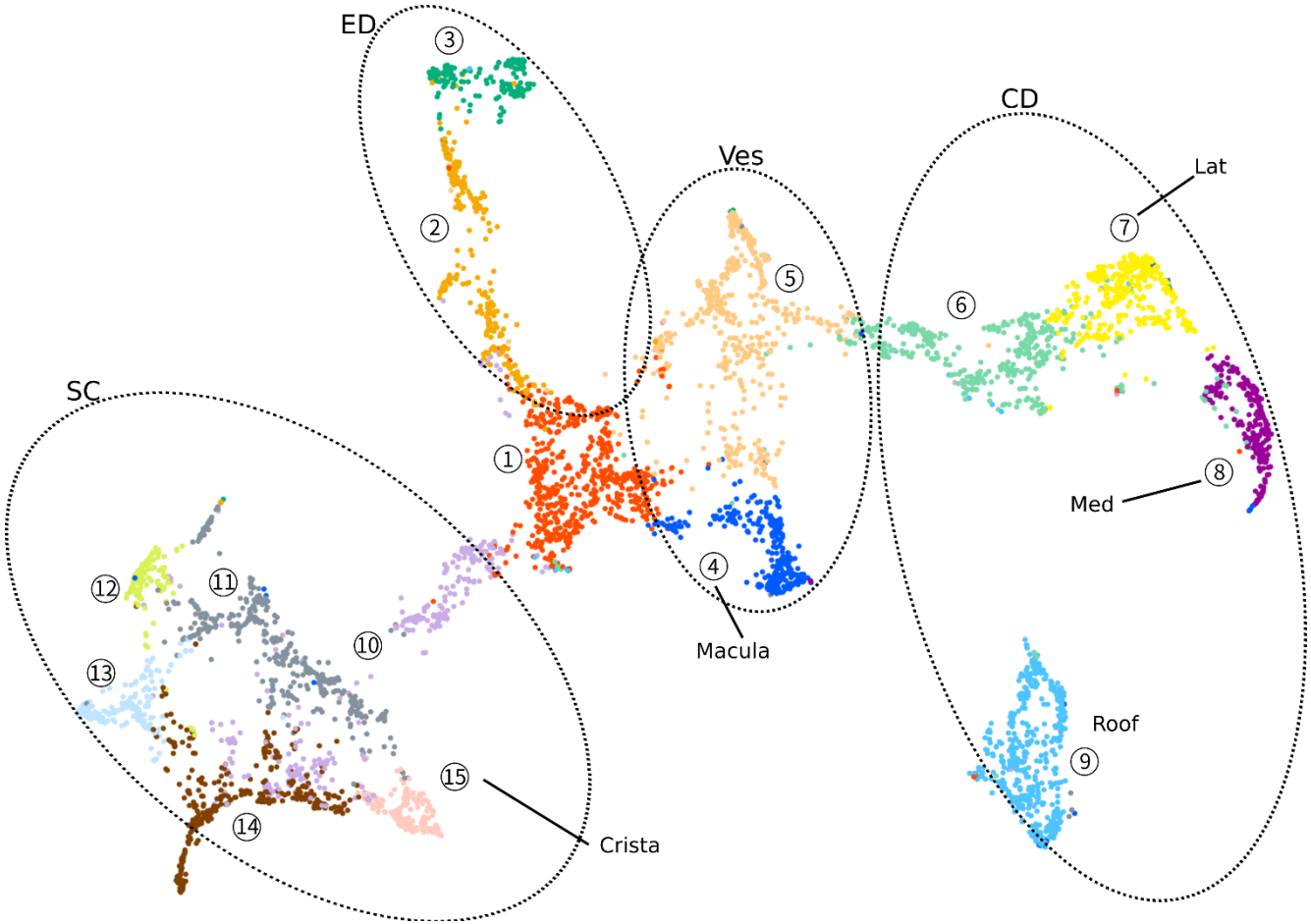
ED
Ves
CD
SC
Lat
Med
Macula
Roof
Crista
1
2
3
4
5
6
7
8
9
10
11
12
13
14
15

Fig. 3

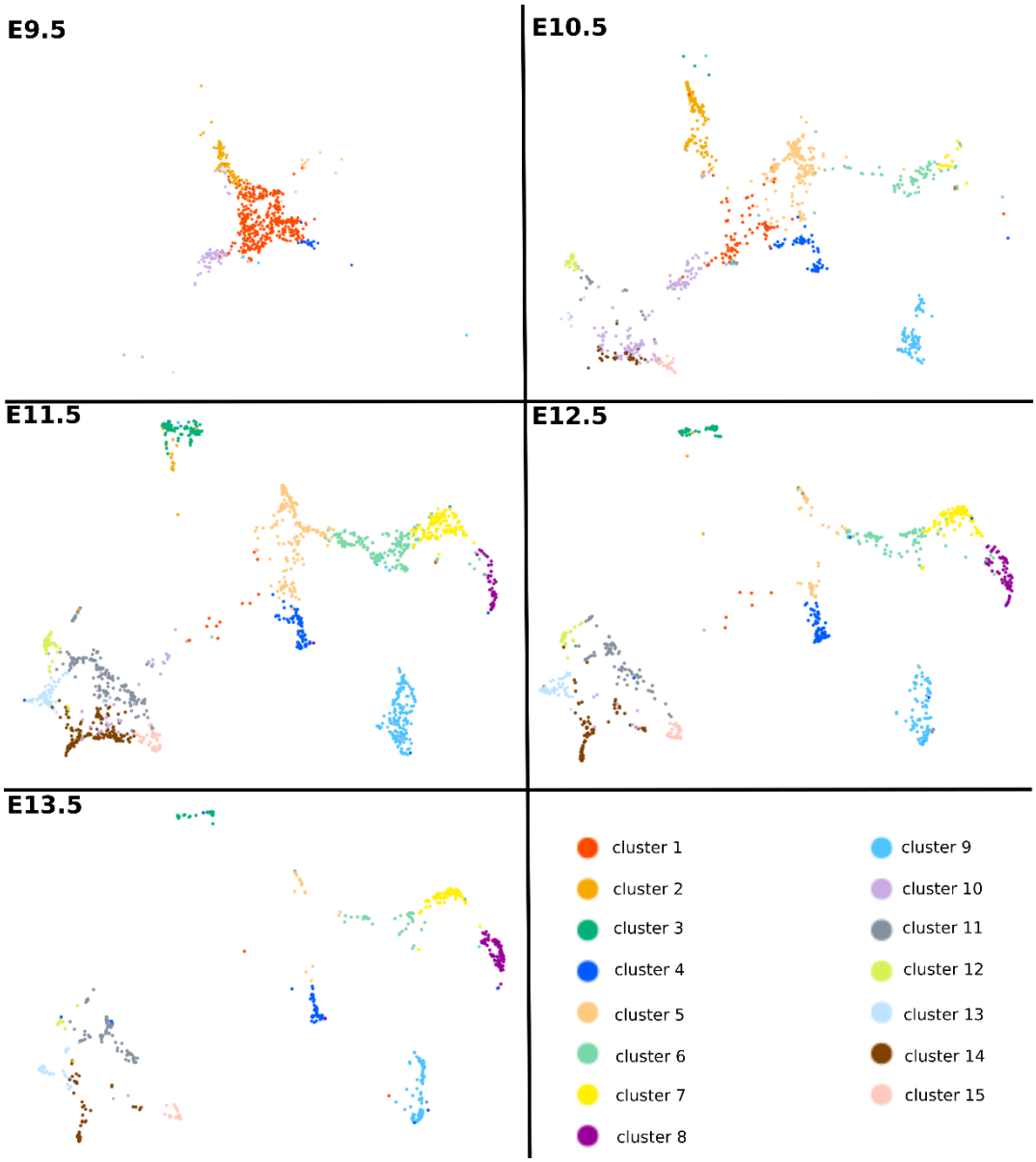
E9.5
E10.5
E11.5
E12.5
E13.5
cluster 1
cluster 2
cluster 3
cluster 4
cluster 5
cluster 6
cluster 7
cluster 8
cluster 9
cluster 10
cluster 11
cluster 12
cluster 13
cluster 14
cluster 15

Fig. 4

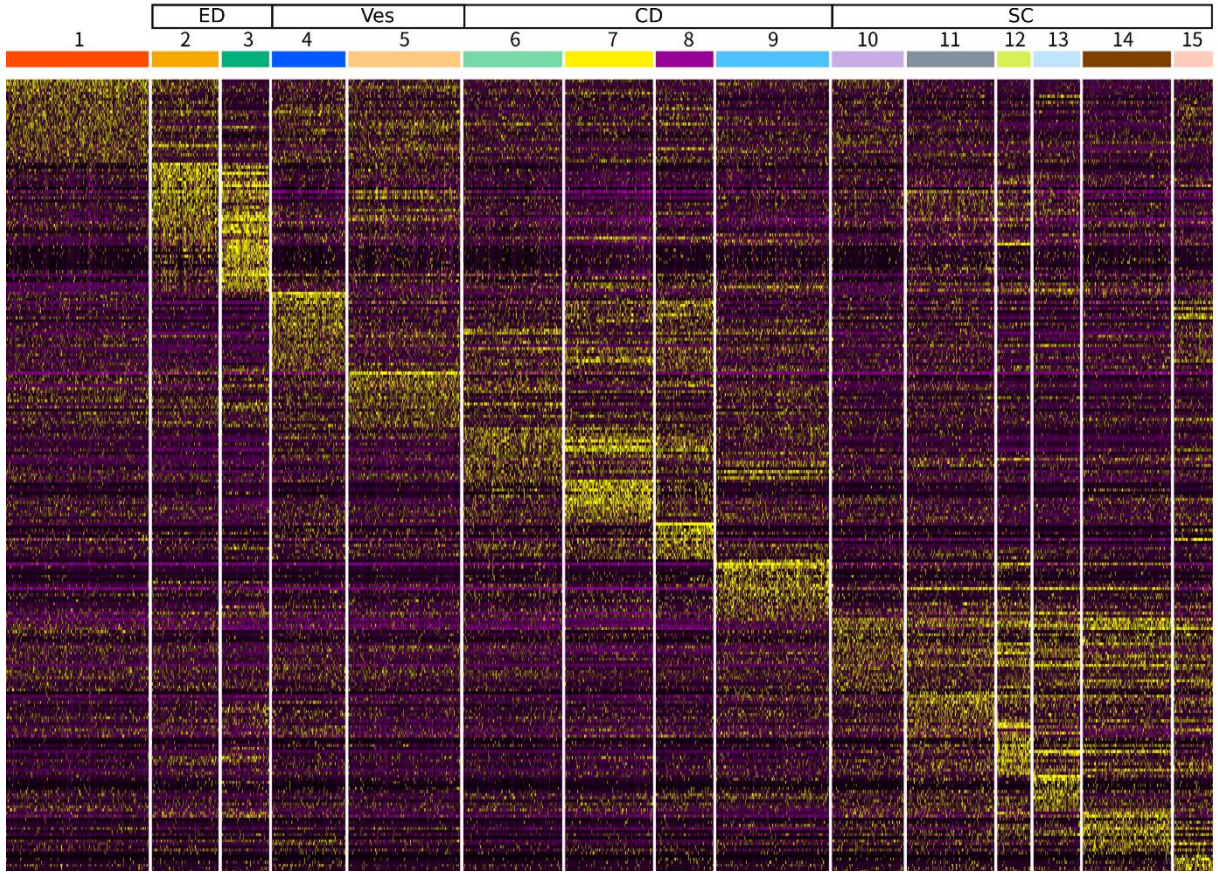

Fig. 5

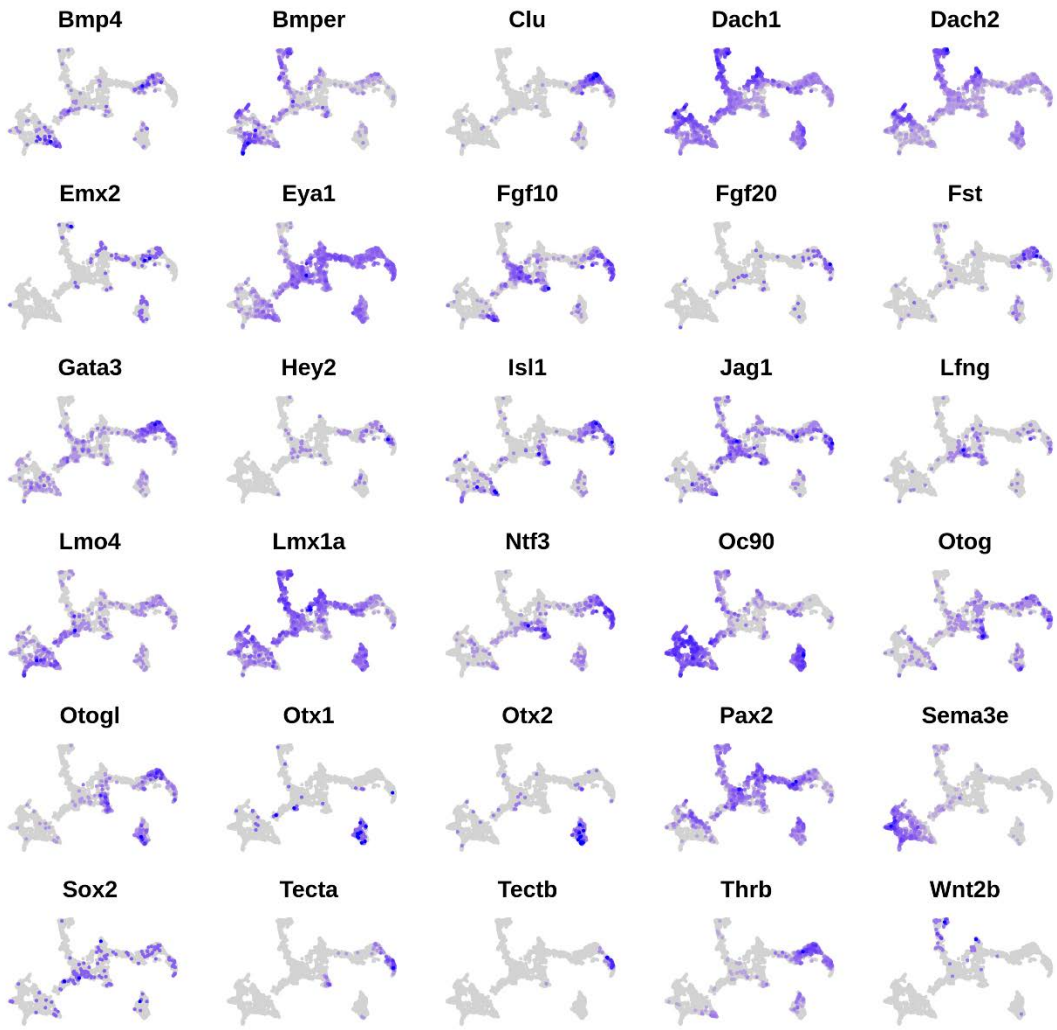
Bmp4
Bmper
Clu
Dach1
Dach2
Emx2
Eya1
Fgf10
Fgf20
Fst
Gata3
Hey2
Isl1
Jag1
Lfng
Lmo4
Lmx1a
Ntf3
Oc90
Otog
Otogl
Otx1
Otx2
Pax2
Sema3e
Sox2
Tecta
Tectb
Thrb
Wnt2b

Fig. 6

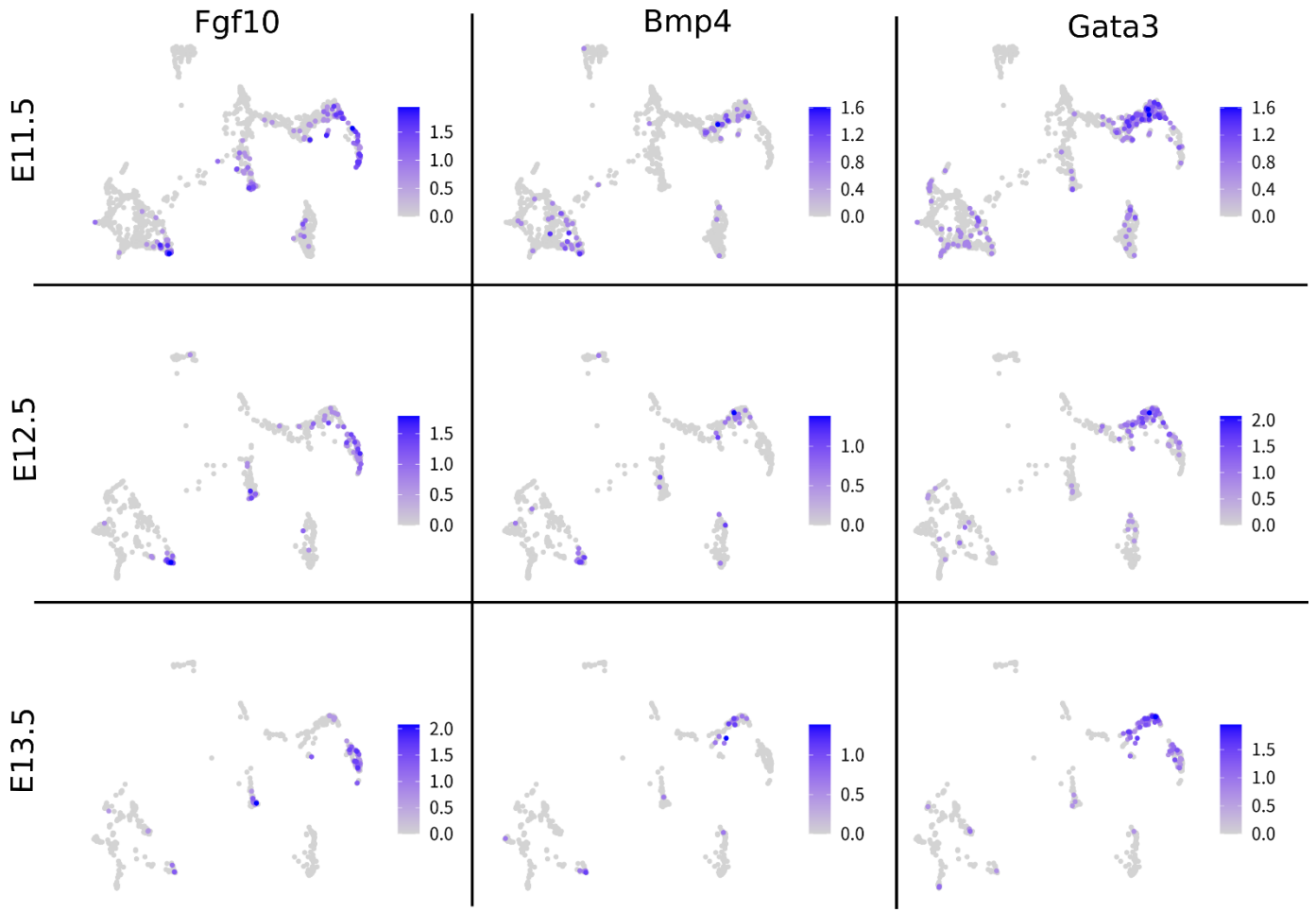

Fig. 7

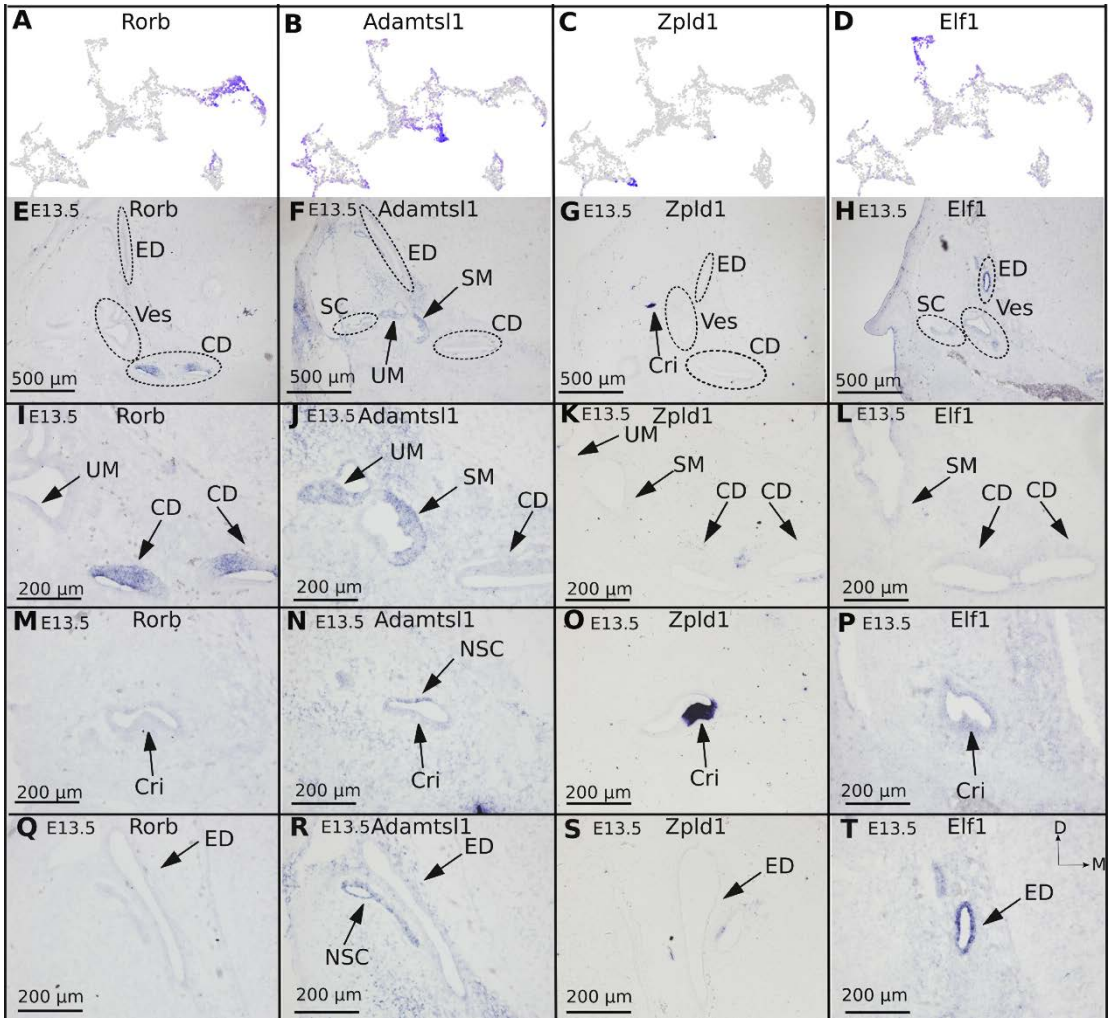
A Rorb
B Adamtsl1
C Zpld1
D Elf1
E E13.5 Rorb
ED
Ves
CD
500 µm
F E13.5 Adamtsl1
ED
SM
SC
CD
UM
500 µm
G E13.5 Zpld1
ED
Ves
CD
Cri
500 µm
H E13.5 Elf1
ED
SC
Ves
500 µm
I E13.5 Rorb
UM
CD
CD
200 µm
J E13.5 Adamtsl1
UM
SM
CD
200 µm
K E13.5 Zpld1
UM
SM
CD CD
200 µm
L E13.5 Elf1
SM
CD CD
200 µm
M E13.5 Rorb
Cri
200 µm
N E13.5 Adamtsl1
NSC
Cri
200 µm
O E13.5 Zpld1
Cri
200 µm
P E13.5 Elf1
Cri
200 µm
Q E13.5 Rorb
ED
200 µm
R E13.5 Adamtsl1
ED
NSC
200 µm
S E13.5 Zpld1
ED
200 µm
T E13.5 Elf1
D
M
ED
200 µm

Fig. 8

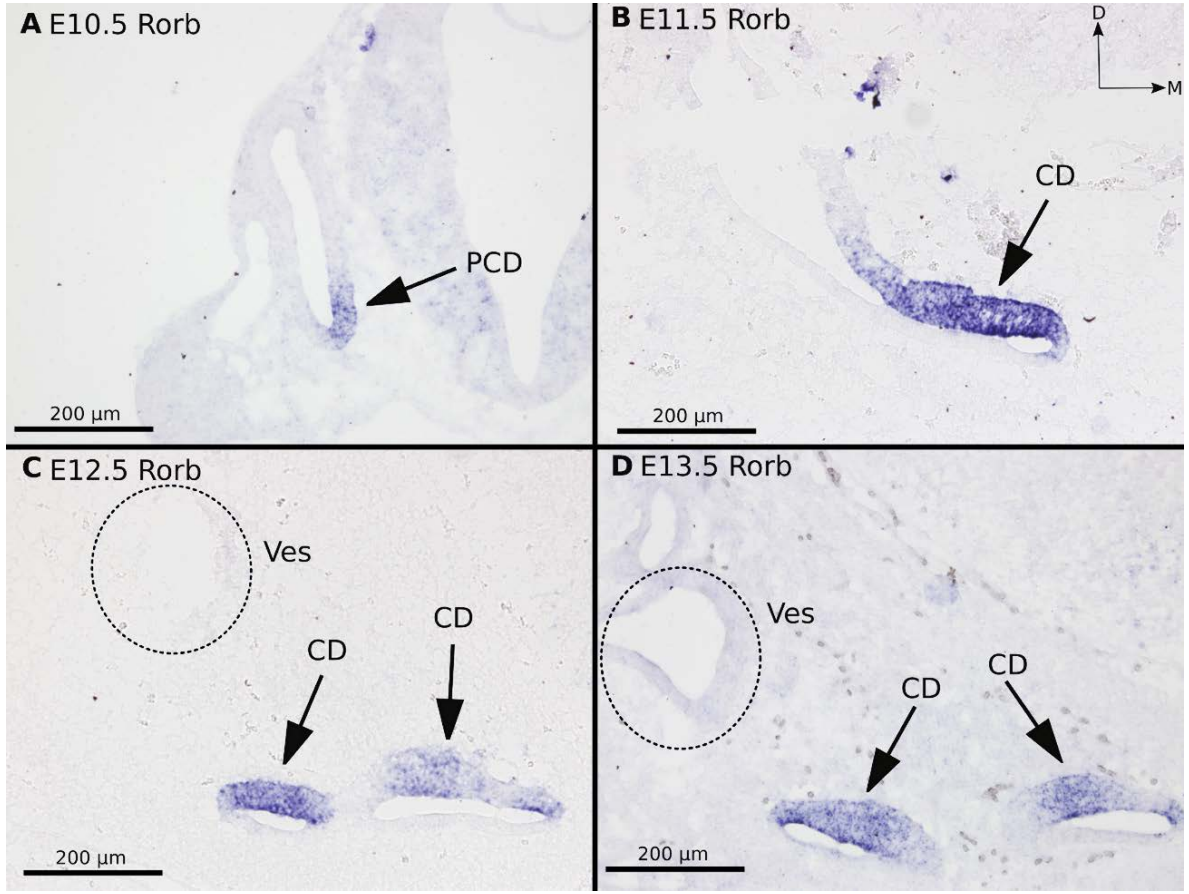
A E10.5 Rorb
PCD
200 µm
B E11.5 Rorb
D
M
CD
200 µm
C E12.5 Rorb
Ves
CD
CD
200 µm
D E13.5 Rorb
Ves
CD
CD
200 µm

Fig. 9

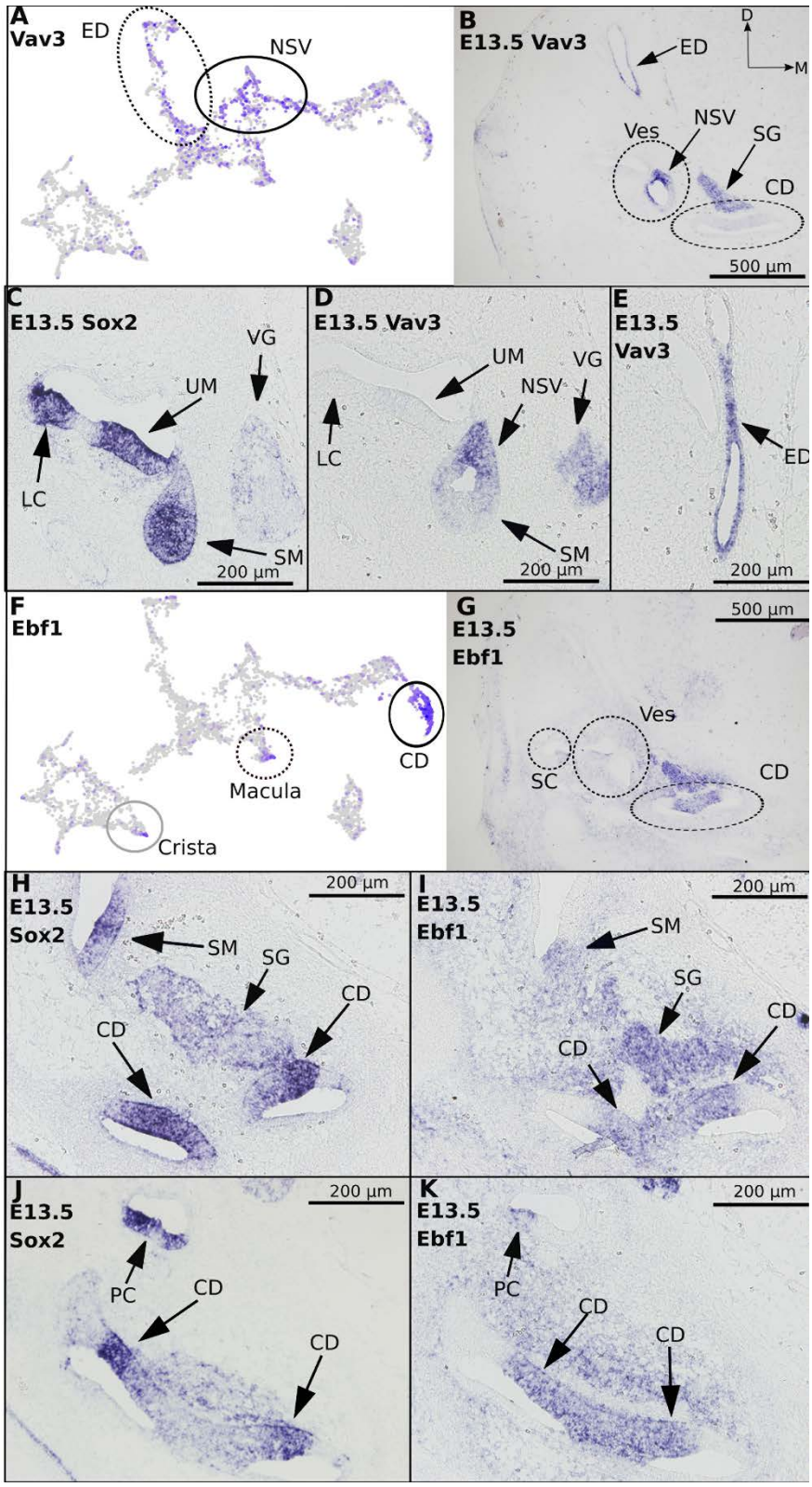
A
Vav3
ED
NSV
B
E13.5 Vav3
D
M
ED
Ves
NSV
SG
CD
500 µm
C
E13.5 Sox2
VG
UM
LC
SM
200 µm
D
E13.5 Vav3
UM
VG
NSV
LC
SM
200 µm
E
E13.5
Vav3
ED
200 µm
F
Ebf1
CD
Macula
Crista
G
E13.5
Ebf1
500 µm
Ves
SC
CD
H
E13.5
Sox2
200 µm
SM
SG
CD
CD
I
E13.5
Ebf1
200 µm
SM
SG
CD
CD
J
E13.5
Sox2
200 µm
PC
CD
CD
K
E13.5
Ebf1
200 µm
PC
CD
CD